Theoretical and Spectroscopic Study of a Series of Styryl-Substituted Terthiophenes

Tracey M. Clarke,[†] Keith C. Gordon,*[,†] David L. Officer,[‡] Simon B. Hall,[‡] Gavin E. Collis,[‡] and Anthony K. Burrell[§]

Department of Chemistry, University of Otago, P.O. Box 56, Dunedin, New Zealand, Nanomaterials Research Centre, IFS—Chemistry, Massey University, Palmerston North, New Zealand, and Los Alamos National Laboratory, P.O. Box 1663, Los Alamos, New Mexico 87545

Received: May 14, 2003; In Final Form: August 25, 2003

Molecular structures of a series of 3′-[1*E*-2-(4-R-phenyl)ethenyl]-2,2′:5′,2″-terthiophenes have been modeled using ab initio calculations. The potential energy surfaces of three important dihedral angles were calculated using the HF/3-21G(d) method. Each dihedral angle is represented by a distinct potential energy surface, while the identity of the R group has only a modest influence. DFT methods (B3LYP/6-31G(d)) were used to calculate the geometry and vibrational spectra of each molecule. Analysis of the theoretical vibrational data reveals numerous conserved modes that are localized on the terthiophene or phenyl groups. There is good agreement between the observed and calculated vibrational spectra of the molecules. Conformational changes have only a minor effect on the spectra. The calculated molecular orbitals, which are supported by electronic absorption measurements, suggest that the first excited state should have charge-transfer features for the molecules with strongly electron withdrawing or donating substituents.

I. Introduction

Since the discovery of conductivity in doped polyacetylene in 1977,[1] conjugated organic polymers have been widely studied. Their unique electronic and optoelectronic properties make them promising materials for a broad range of applications. Field-effect transistors,[2] OLEDs,[3] and plastic photovoltaic cells[4,5] with polymeric active layers are currently being investigated. Polythiophenes are an example of the type of conducting polymers that have been used in these applications. These polymers, prepared from thiophene and its oligomers, such as terthiophene, are known for their simple functionalization, p-type semiconductor properties, and relatively good stability in air for both the neutral and oxidized states.[6,7]

However, the efficiency of plastic photovoltaic cells needs to be improved before they are commercially viable. To date, fabrication of devices with energy conversion efficiencies of up to 2.5% in sunlight has been achieved.[8] Further enhancements in efficiency will require elucidation of the precise mechanism of conduction in conjugated polymers, which, in turn, will lead to a more rational design of these polymers and therefore increase the efficiency of the resultant devices. To address this issue, the precise electronic structure of the required polymer must be established. However, electronic structure determinations of polymers present a number of difficulties, due to their amorphous structures and polydispersity. To overcome these difficulties, oligomers are often used to model the polymer structure. This technique has been termed the oligomeric approach and is a reasonable method, since the effective conjugation length in disordered polymers is short—approximately 6−12 monomer units.[7] Also, in contrast to polymers, short oligomers can be well defined in their physical and chemical properties. Structure/property relationships of these oligomers, such as the connection between molecular orbital characteristics and conductivity, can be ascertained from this method and extrapolated to the polymer system.[9,10] The use of functionalized terthiophenes in particular as the oligomer has a number of experimental advantages. Terthiophene has a lower oxidation potential than thiophene or bithiophene; thus, electrochemical polymerization is easier. Additionally, the polymers generated from terthiophene form a more ordered structure than those synthesized from thiophene.[11] This results in greater charge carrier mobility. The functionalization (usually alkyl substitution) is required in order to impart solubility and processibility to the polymer.

Modeling the structure of terthiophenes and other oligothiophenes often involves ab initio calculations in conjunction with vibrational spectroscopy, an important tool for characterizing the structural properties of these molecules. The use of ab initio calculations to simulate infrared and Raman spectra is a well-known and often utilized technique. Geometry optimizations are performed, from which calculated vibrational spectra are derived. These predicted spectra are compared to the experimental spectra, and if this comparison is favorable, then it is reasonable to assume that the calculated optimized structure is a reliable model of the true structure. Once the veracity of the ab initio calculations has been checked in this manner, they can be used to derive important structural and electronic parameters, such as the nature of the molecular orbitals.

Oligothiophenes' flexible backbones and their resultant low rotational energy barriers suggest that a number of different conformations can exist in solution at room temperature. Evidence for syn-gauche and anti-gauche conformers has been obtained from NMR spectra,[12,13] electron diffraction studies,[14] and fluorescence excitation spectra[15] for bithiophene. In the solid state, however, crystal packing forces become significant and the anti coplanar conformation is observed.[16] Quantum chemical calculations have therefore been performed on a variety of thiophene-based systems in order to investigate conformation.[17−26]

* Corresponding author. E-mail: kgordon@alkali.otago.ac.nz.
[†] University of Otago.
[‡] Massey University.
[§] Los Alamos National Laboratory.

10.1021/jp030619y CCC: $25.00
Published on Web 11/27/2003

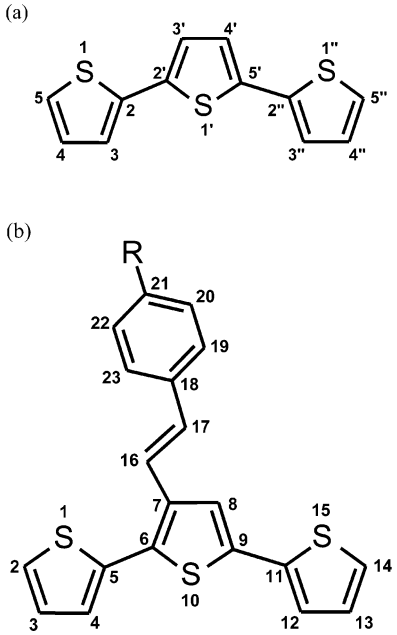

Figure 1. Numbering system for 2,2′:5′,2″-terthiophene, which can be reduced or extended for shorter and longer oligothiophenes, respectively (a). The structure of R-pet, where R = $-NMe_2$, $-NH_2$, $-OMe$, $-H$, $-CN$, and $-NO_2$ (b). The atom numbering in part b corresponds to that used in Table 1 and for the description of the dihedral angles, where ϕ_1 = (S1,C5,C6,S10), ϕ_2 = (S10,C9,C11,S15), and ϕ_3 = (C8,C7,C16,C17).

The potential energy surface and rotational energy barriers of the bithiophene inter-ring dihedral angle, S1,C2,C2′,S1′ (from the numbering system of a generalized oligothiophene shown in Figure 1a), have been reported using both semiempirical and ab initio methods. Hartree−Fock (HF) calculations using the 3-21G(d) or 6-31G(d) basis sets show a global energy minimum at 148° (the anti-gauche geometry) and a local energy minimum at 42−44° (syn-gauche).[18,19] This potential energy surface is consistent with the electron diffraction results, which found the anti-gauche geometry (148 ± 3°) to be more prevalent than the syn-gauche (36 ± 5°).[14] The omission of polarization functions (HF/3-21G, for instance) leads to an energy surface in which the planar anti conformation is the global minimum and the rotational energy barrier is significantly overestimated. Semiempirical methods, such as MNDO and AM1, also fail to represent conformational properties accurately and underestimate the barriers.[19] Conversely, including the effects of electron correlation provides qualitatively the same curve as the HF calculations,[18] with the exception being the height of the energy barriers. B3LYP/6-31G(d), for example, gives lower barriers to planarity (0° and 180°) and a larger barrier between the two energy minima (90°).[17,20] DFT methods such as this one do not correlate with the experimental evidence as well as the ab initio methods MP2 and HF.[21,22]

The potential energy surface calculated for terthiophene (using Hartree−Fock) possesses the global energy minimum at 148° and a local minimum at 44°, identical to the case of bithiophene.[23,24] HF/3-21G(d) and HF/6-31G(d) calculations provide very similar energy barrier values, which are consistently larger than those found in bithiophene. The B3LYP/6-31G(d) method has also been applied to terthiophene,[17] and the same trends present for bithiophene are observed.

The conformational properties of substituted bithiophenes,[19,25] terthiophenes,[23] and longer oligothiophenes[26] have also been reported. It was discovered that substitution of one methyl group at the 4- or 5-position of bithiophene has little to no effect on the potential energy surface, but substitution at the 3-position (Figure 1a) has a marked effect.[19,25] The energy minima of the inter-ring dihedral angle (S1,C2,C2′,S1′) shift to more twisted conformations, from 148° to 119° and 44° to 57°. In addition, the energy barrier between the two minima decreases considerably, and the syn-gauche geometry becomes slightly preferred over the anti-gauche. The energy barriers against planarity increase (the exact values of which are dependent upon the computational method).[25] Changing the substituent to the larger ethyl group exacerbates this effect. Disubstitution of bithiophene involving the 3-position also has a pronounced effect on the potential energy surface, as demonstrated by HF/3-21G(d) and HF/6-31G(d,p) calculations of 3,3′-dimethyl-2,2′-bithiophene and 3,4′-dimethyl-2,2′-bithiophene.[27] Only a single energy minimum exists for both molecules (in contrast to unsubstituted and monosubstituted bithiophenes): at 94° for 3,3′-dimethyl-2,2′-bithiophene and 109° for 3,4′-dimethyl-2,2′-bithiophene. In the case of 3,4′-dimethyl-2,2′-bithiophene, the energy barriers against planarity are comparable to those seen for monosubstituted bithiophenes, while those of 3,3′-dimethyl-2,2′-bithiophene are considerably higher. Similar results for 3,3′-dimethyl-2,2′-bithiophene were observed by Alemán et al. using the 6-31G(d) basis set.[19]

A number of early calculations on the vibrational properties of thiophene and bithiophene focused on the semiempirical MNDO method and obtained reasonable correlations between experimental and theoretical data.[28,29] Deuteration was used in one instance to confirm the reliability of the calculations.[28] The vibrational spectra of various oligothiophenes have also been measured and analyzed using ab initio calculations; these include thiophene,[30] bithiophene,[31] terthiophene,[32] and longer oligomers up to octithiophene.[33,34] Substituted sexithiophene,[35] polythiophene,[36] and a series of thiophene-based oligomers containing ethenyl linkages[37−39] have also been investigated. DFT methods are most commonly utilized for these systems and are often combined with the basis set 6-31G(d) or 6-31G(d,p). In general, the agreement between these experimental and calculated vibrational spectra is good, indicating that these methods are appropriate for thiophene-based molecules.[36]

The purpose of this work is to model the electronic structures of a series of substituted terthiophenes, 3′-[1*E*-2-(4-R-phenyl)-ethenyl]-2,2′:5′,2″-terthiophene (referred to as R-pet hereafter), in which the substituent R varies in terms of its electron withdrawing capacity. The generalized structure of the R-pet molecule is depicted in Figure 1b. The following R groups are investigated, in order from the strongest electron donator: $-NMe_2$, $-NH_2$, $-OMe$, $-H$, $-CN$, and $-NO_2$. The pyridyl derivative, 3′-[1*E*-2-(4-pyridyl)ethenyl]-2,2′:5′,2″-terthiophene (pyr-et), is also examined. The structure modeling will be accomplished using the strategy discussed above: the use of ab initio calculations in conjunction with experimental vibrational spectroscopy. Since the considerable conformational freedom of oligothiophenes has been well documented,[17,18] the first step is to address the conformational properties of these terthiophenes. The second step is to calculate the molecular structures and evaluate the veracity of these ab initio calculations by comparison of the theoretical vibrational spectra with experimental spectra. The final step is to examine the electronic structures that the calculations have produced and use the molecular orbitals to infer conductivity characteristics.

II. Experimental Section

The synthesis and purification methods of the R-pet compounds are described elsewhere.[40]

Spectral Measurements. FT-IR spectra were recorded using a Perkin-Elmer Spectrum BX FT-IR system on sample solutions ($CDCl_3$) contained in a transmission cell with CaF_2 windows and a 0.5 mm path length. FT-Raman spectra were recorded from solid powder samples using a Bruker IFS-55 FT-interferometer bench equipped with an FRA/106 Raman accessory and a GaAs D425 Raman detector. Radiation of 1064 nm from a Nd:YAG laser with an operating power of 100 mW was utilized for Raman excitation. All FT-IR and FT-Raman spectra were collected after six scans at a resolution of 4 cm^{-1}. Electronic absorption spectra were measured of $\sim 1.1 \times 10^{-5}$ mol L^{-1} solutions in CH_2Cl_2 at room temperature from 250 to 600 nm on a Varian Cary 500 Scan UV−Vis−NIR spectrophotometer using Cary WinUV Scan Application software. Spectra were analyzed using GRAMS 5.0 (Galactic Industries).

Computational Methods. Conformational analyses were performed using the ab initio Hartree−Fock level and the 3-21G(d) basis set and implemented with the PC Spartan Pro software package.[41] Potential energy surfaces were determined by varying the required dihedral angle in 30° increments between the two planar conformations (syn and anti). At each increment, the required dihedral angle was fixed and the rest of the molecule optimized. The vibrational frequencies and the corresponding IR and Raman intensities were calculated using DFT calculations (the B3LYP functional and 6-31G(d) basis set) and the Gaussian 98 program,[42] following geometry optimizations with the same method. Visualization of the vibrational modes and molecular orbitals was provided by the Molekel[43] and Molden[44] programs, respectively. The initial geometry used for the geometry optimizations and frequency calculations had anti-gauche terthiophene inter-ring dihedral angles and the (C8,C7,C16,C17) dihedral angle at ∼17°. The geometry optimizations were performed with no constraints on planarity. As previously recommended for B3LYP/6-31G(d) calculations, a scale factor of 0.96 was applied to all predicted frequencies.[45]

III. Results and Discussion

III.a. Conformation. Steric effects and conjugation determine conformation in oligothiophenes. Steric interactions between the rings are unfavorable and would result in a twisted structure if not for the decrease in energy that planarity and the ensuing conjugation impart. This balance usually results in rotational energy maxima at 0°, 90°, and 180° and energy minima at approximately 150° and 45°.[17,24,46] The rotational energy barriers of R-pet were examined to establish which conformation, if any, is particularly energetically favorable and therefore should be used in further geometry optimizations and frequency calculations. The method HF/3-21G(d) was utilized for these conformational analyses. It has been reported that the Hartree−Fock method provides potential energy surfaces consistent with experimental observations,[18] in contrast to semiempirical[19] and DFT[20] methods. In addition, polarization functions are essential to provide an accurate representation of the energy barriers present in oligothiophenes.[18,19] The potential energy surface of terthiophene was calculated in order to assess whether the 3-21G(d) basis set (the smallest standard basis set to include polarization functions) is large enough to investigate these molecules accurately. The predicted energy maxima and minima are very close to those calculated using the larger basis sets 6-31G(d) and 6-31G(d,p) (as previously observed for bithiophene).[18] Therefore, the 3-21G(d) basis set was concluded to be satisfactory for these conformational analyses,[23] in that it should be reasonably accurate while being efficient to calculate.

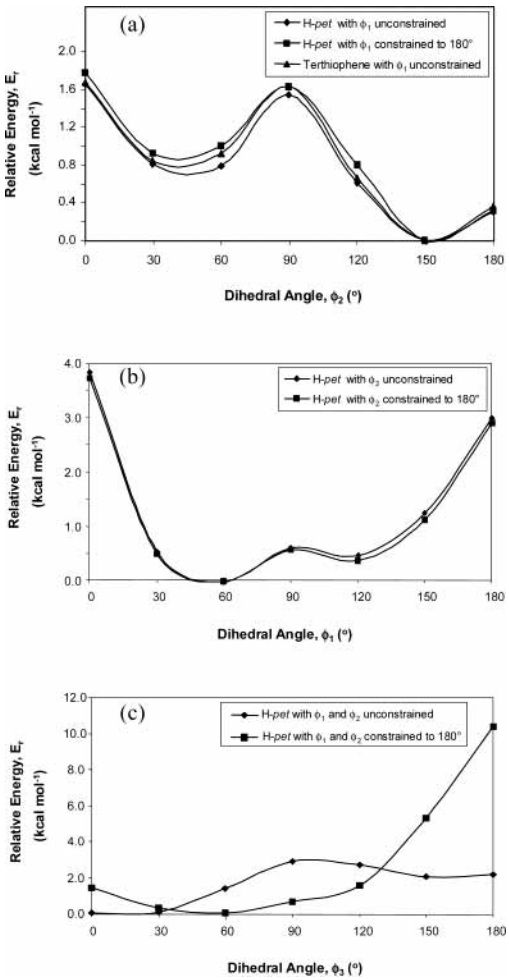

Figure 2. Fitted potential energy surfaces of dihedral angles ϕ_2 (a), ϕ_1 (b), and ϕ_3 (c) of H-pet calculated using the HF/3-21G(d) method for both approaches (constrained, ■; and unconstrained, ◆), as described in the text. The potential energy surface of ϕ_2 of terthiophene, also calculated using HF/3-21G(d), is shown in part a for comparison.

Three dihedral angles of R-pet are important due to their high degree of rotational flexibility. These are denoted ϕ_1 (S1,C5,C6,S10), ϕ_2 (S10,C9,C11,S15), and ϕ_3 (C8,C7,C16,C17), where ϕ_1 and ϕ_2 are associated with the terthiophene inter-ring bonds and ϕ_3 with the bond connecting the terthiophene to the phenyl ethenyl substituent (Figure 1b). To calculate the potential energy surface of the simplest molecule, H-pet, two approaches were used. The first of these (applied to ϕ_1, ϕ_2, and ϕ_3) was to change the required angle and allow all other angles free rotation. The second approach (for ϕ_1 and ϕ_2) was to alter the required angle and permit free rotation for all other angles except for the other inter-ring dihedral angle, which was constrained to 180°. In the case of ϕ_3, both terthiophene inter-ring dihedral angles, ϕ_1 and ϕ_2, were unconstrained in the first approach and constrained to 180° in the second. This method allows interdependence between angles to be observed.

All calculated potential energy surfaces for both approaches (HF/3-21G(d)) are displayed in Figure 2. The dihedral angle ϕ_2 for H-pet possesses a predicted potential energy curve that has a very similar shape to that of terthiophene with energy maxima at 0, 90, and 180°.[23,24] The global minimum is at approximately 150°, and a local minimum is at about 45°. The energy barrier to rotation (rotating past 90°) is 1.54 kcal mol^{-1} when no other angles are constrained, and the energy barriers against planarity are 1.66 kcal mol^{-1} (0°) and 0.30 kcal mol^{-1} (180°). The first two of these barriers are considerable when

the value of kT at room temperature (0.59 kcal mol^{-1}) is taken into account. These barriers are comparable to those of terthiophene, which are 1.63, 1.68, and 0.36 kcal mol^{-1}, respectively (Figure 2a). The close similarities between the potential energy curves of unsubstituted terthiophene and H-pet's ϕ_2 suggest that the presence of the substituent in H-pet has no significant effect on the rotational barriers of ϕ_2. This is not an unexpected observation, since ϕ_2 is separated spatially by a considerable distance (>5 Å) from the substituent. Substitution at the 4-position of an oligothiophene (Figure 1a) is known to have little effect on the potential energy surface of the (S1,C2,C2′,S1′) inter-ring dihedral angle.[25,26]

The potential energy surface of ϕ_2 is slightly sensitive to ϕ_1, as discovered when the second approach was applied. When ϕ_1 is fixed at 180°, the ϕ_2 surface shows a small increase in energy (a maximum of 0.21 kcal mol^{-1}). In addition, the alteration of ϕ_2 causes only slight changes in ϕ_1 (120−125°) when ϕ_1 is not constrained. Therefore, these two dihedral angles are not strongly dependent upon one another.

The potential energy surface of H-pet along the ϕ_1 degree of freedom, however, is significantly different compared to that of ϕ_2. The energy barriers against planarity are substantially higher (3.79 and 2.96 kcal mol^{-1}). This is attributable to the effect of the large phenyl ethenyl substituent, which is in the 3-position relative to ϕ_1 and thus is much closer to this dihedral angle (2−3 Å) than it is to ϕ_2. Substitution at this position therefore causes the destabilization of the two planar conformations due to increased steric interactions.[25,26] The shape of the curve is also different: the global minimum is now located at approximately 50°, and 120° is a local minimum. These angles are much more twisted (closer to 90°) than that observed in unsubstituted terthiophene. This also occurs as a result of the substituent's steric effect. The syn-gauche and anti-gauche conformations are much closer in energy for ϕ_1 (0.47 kcal mol^{-1}) than they are for ϕ_2. The energy barrier between the two conformations is 0.60 kcal mol^{-1}, which is significantly lower than that of ϕ_2 and comparable to kT at room temperature. These findings indicate that both geometries will exist experimentally for this dihedral angle and that they will be rapidly interconverting at room temperature (the syn-gauche conformation is slightly preferred). Conversely, because of its higher 90° energy barrier and larger energy difference between the two minima, ϕ_2 is expected to be predominantly anti-gauche. The existence of a global minimum for ϕ_1 at 50° rather than 120° is due to steric considerations: by adopting the syn-gauche arrangement, the bulky sulfur atom of the terthiophene ring and the closest ethenyl hydrogen are as far from each other as possible. Global energy minima at 40−60° with low energy barriers to rotation and high barriers against planarity have been observed in other substituted oligothiophenes.[19,23,25]

It was also observed that the potential energy surfaces of ϕ_1 are virtually identical whether or not ϕ_2 is constrained to 180°. Changing ϕ_1 from 0 to 180° while allowing ϕ_2 free rotation shows that ϕ_2 consistently remains at approximately the same angle (146−148°). It can be concluded, therefore, that ϕ_1 and ϕ_2 are not strongly interdependent (as observed from the ϕ_2 surface as well). However, altering the value of ϕ_1 causes ϕ_3 to vary considerably; thus, these two dihedral angles are dependent on one another. When ϕ_1 is planar, ϕ_3 is approximately 50°, and when ϕ_1 is 90°, ϕ_3 is almost planar.

The dihedral angle ϕ_3 exhibits the highest energy barrier to rotation when no other angles are constrained, at a value of 2.85 kcal mol^{-1}. Again, the cause of this barrier is probably steric hindrance, as evidenced by twisted ϕ_1 values. Thus, discrete conformers are expected that do not interconvert at room temperature. The global minimum is at 0°, and a shallow local minimum is located at 150°. Due to the relatively high energy difference between the two minima (2.00 kcal mol^{-1}), the conformer containing $\phi_3 = 0°$ is predicted to be the favored geometry experimentally, and it is unlikely that a high proportion of the other conformer ($\phi_3 = 150°$) will exist.

However, when both ϕ_1 and ϕ_2 are constrained to 180°, the potential energy curve of ϕ_3 changes appreciably. Since the terthiophene unit is completely planar, when ϕ_3 is also planar (180°), unfavorable steric interactions result between the substituent and the closest thiophene ring, thus significantly increasing the energy of this geometry (relative to the unconstrained situation). The lowest energy occurs when ϕ_3 is twisted with respect to the case of the terthiophene, thus minimizing the steric hindrance. Hence, ϕ_3 is strongly dependent upon the geometry of the terthiophene group.

The potential energy surfaces of NO_2-pet and NMe_2-pet were also determined in order to establish the effect, if any, of the substituent (Figure 1S). The potential energy surface along the ϕ_3 degree of freedom shows the most significant variation. This was expected, since this dihedral angle is spatially closest to the R group. The shapes of the three curves are identical, but NO_2-pet has the largest energy barrier to rotation (0.51 kcal mol^{-1} higher than H-pet). The only other difference of note is NMe_2-pet's possession of the lowest energy local minimum (150°). The other two dihedral angles, ϕ_1 and ϕ_2, show less variation between the three molecules, and their energy surfaces are very similar, especially for ϕ_2. The main difference in the ϕ_1 curves is in the heights of the energy barriers against planarity, where NO_2-pet has the highest and NMe_2-pet the lowest, with a difference of 0.66 (0°) and 0.68 (180°) kcal mol^{-1} between the two.

In the particular case of R-pet, the controlling influence on conformation appears to be the steric considerations between the terthiophene unit and the substituent. This interaction results in a preference for ϕ_1 to adopt either the anti-gauche or the syn-gauche arrangement (with a negligible energy barrier between the two) and ϕ_3 to be slightly nonplanar ($\sim$ 17°, B3LYP), while the more spatially distant ϕ_2 follows the terthiophene pattern and favors an anti-gauche geometry. Therefore, this approximate conformation (with $\phi_1 \sim \phi_2 \sim$ anti-gauche, for simplicity) was then used for the higher-level geometry optimizations and frequency calculations.

III.b. Geometry. Geometry optimizations were performed with the B3LYP/6-31G(d) method. The resulting geometries are very similar throughout the series of molecules. Bond lengths (as shown in Table 1) and angles are consistent in the terthiophene and ethenyl units but vary in the phenyl bonds. The two phenyl bonds directly adjacent to the R group differ the most, depending on the identity of that group, although there appears to be no trend linking electron withdrawing capacity to the change in bond lengths. NMe_2-pet has the longest bonds (1.417 Å), while pyr-et has the shortest (1.339 Å). The phenyl bond angles also vary more than the terthiophene's, but only by a maximum of 2.4°. The dihedral angle ϕ_1 ranges from 138.8° to 141.7°, the angle ϕ_2 from 164.7° to 167.7°, and the angle ϕ_3 from 15.7° to 17.7°. The propensity of the B3LYP level of theory to overestimate the importance of electronic conjugation contributions is evident from these results, in which the less hindered ϕ_2 is more planar than observed experimentally in other oligothiophenes (148°).[14]

In the case of NMe_2-pet, B3LYP/6-31G(d) geometry optimizations for two conformations were performed, in preparation

TABLE 1: Optimized Bond Lengths of All R-pet Molecules Calculated Using the B3LYP/6-31G(d) Method

bond	NO_2-pet	CN-pet	pyr-et	H-pet	MeO-pet	NH_2-pet	NMe_2-pet
C2−C3	1.369	1.369	1.369	1.369	1.369	1.368	1.368
C3−C4	1.422	1.422	1.422	1.422	1.422	1.422	1.422
C4−C5	1.381	1.381	1.381	1.381	1.381	1.381	1.381
C5−C6	1.452	1.452	1.452	1.452	1.452	1.451	1.451
C6−7	1.395	1.395	1.394	1.394	1.394	1.394	1.395
C7−8	1.432	1.432	1.432	1.432	1.432	1.432	1.432
C8−9	1.372	1.372	1.372	1.373	1.372	1.372	1.372
C9−C11	1.449	1.449	1.449	1.449	1.449	1.449	1.449
C11−C12	1.379	1.379	1.379	1.379	1.379	1.379	1.379
C12−13	1.423	1.423	1.423	1.424	1.424	1.424	1.424
C13−C14	1.368	1.368	1.368	1.368	1.368	1.368	1.368
C7−C16	1.455	1.456	1.456	1.458	1.458	1.457	1.457
C16−C17	1.352	1.352	1.351	1.351	1.351	1.352	1.353
C17−C18	1.461	1.462	1.463	1.465	1.462	1.460	1.459
C18−C19	1.411	1.410	1.406	1.408	1.411	1.408	1.407
C19−C20	1.389	1.388	1.393	1.393	1.386	1.389	1.388
C20−C21	1.394	1.405	1.339	1.395	1.402	1.405	1.413
C21−C22	1.397	1.408	1.342	1.399	1.402	1.408	1.417
C22−C23	1.386	1.386	1.391	1.391	1.393	1.386	1.386
C18−C23	1.412	1.411	1.407	1.409	1.406	1.410	1.409
C2−S1	1.732	1.732	1.732	1.732	1.733	1.733	1.733
C5−S1	1.761	1.761	1.761	1.761	1.762	1.762	1.762
C6−S10	1.753	1.753	1.754	1.756	1.757	1.757	1.758
C9−S10	1.756	1.755	1.755	1.755	1.754	1.754	1.754
C11−S15	1.756	1.756	1.757	1.757	1.757	1.757	1.757
C14−S15	1.735	1.735	1.735	1.735	1.735	1.735	1.735

for subsequent investigations of the conformational dependence of the theoretical vibrational spectra (vide infra). The first conformer has ϕ_3 approximately equal to 150° (conformer 1), and the second has this angle at 15−18° (conformer 2), according to the two energy minima seen for this dihedral angle. In both of these conformers, ϕ_1 and ϕ_2 are anti-gauche. Additionally, three conformations of NO_2-pet were calculated, where conformer 3 has ϕ_1 in a syn-gauche arrangement instead of anti-gauche. Since a relatively small rotational energy barrier separates these two conformations that differ in ϕ_1, both minima of ϕ_1 were examined.

For both NO_2-pet and NMe_2-pet the large ϕ_3 values of conformer 1 (∼150°) force ϕ_1 to twist more significantly toward 90°. As a result, this geometry has a higher calculated energy than conformer 2, thus confirming the latter's higher stability. However, the energy difference between these conformers is less for NMe_2-pet (3.14 kcal mol^{-1}) than it is for NO_2-pet (5.02 kcal mol^{-1}). This supports the results of the previous section, where it was found from the ϕ_3 potential energy surface that NMe_2-pet has a lower energy difference than NO_2-pet between conformers 1 and 2, while NO_2-pet has a higher energy barrier between the conformers. This may imply that NMe_2-pet is more likely to reveal evidence of both conformations experimentally. The calculated energies of conformers 2 and 3 of NO_2-pet show that conformer 3 is the more stable form by only 0.63 kcal mol^{-1}. This small energy difference between the syn-gauche and anti-gauche geometries of ϕ_1 reflects its potential energy surface calculated in the previous section.

The X-ray crystal structures of R-pet have not yet been reported. However, the crystal structures of related compounds, such as unsubstituted oligothiophenes, have shown that the anti-coplanar conformation is particularly common in the solid state.[47−49] Numerous instances of anti-gauche[50,51] and a few syn-gauche[52] geometries have also been reported, particularly for the alkyl-substituted and end-capped compounds. The low energy barrier between the anti-gauche and syn-gauche minima of ϕ_1 is supported by the crystal structure of 3′-methyl-2,2′:5′,2″-terthiophene,[52] which has the same substitution pattern as R-pet. It was found that disorder between the two orientations existed and that the occupancy of two sites by a sulfur and a carbon atom was equal.

III.c. Vibrational Spectra. The optimized structures of R-pet discussed in the previous section were used to calculate the predicted vibrational spectra with the B3LYP functional and 6-31G(d) basis set. Comparison of these calculated spectra with experimentally obtained IR and Raman spectra shows, in general, a close correspondence with small average root-mean-square (rms) values. NO_2-pet possesses the largest average rms value (10 cm^{-1}), while pyr-et has the smallest (7 cm^{-1}). Considering the accuracy and resolution of the spectrometers used in this study (1 and 4 cm^{-1}, respectively), this indicates a close correlation between the theoretical and measured spectra. Relative intensities are also in general agreement. Table 2 contains the mode correlation for all of the experimental and calculated data. The theoretical and measured Raman and IR spectra of CN-pet are shown in Figure 3 as an example.

Because the range of molecules considered in this work are structurally closely related, a number of vibrational normal modes are expected to be the same and thus occur at comparable frequencies. The eigenvectors were compared between the molecules for each mode, and numerous matches were established. It was therefore confirmed that the majority of the calculated modes in the region of interest (950−1700 cm^{-1}) were conserved throughout the R-pet series. This mode conservation was also observed experimentally. The eigenvectors of selected modes that usually possess large intensity are displayed in Figure 4 for CN-pet.

Due to the relatively large size of these molecules, their normal modes are complex and involve the movement of numerous atoms. As such, most R-pet modes contain contributions from each group within the molecule, although one group usually vibrates more strongly than the others. This results in distinct phenyl, terthiophene, and ethenyl-based modes. One mode that is completely delocalized, assigned as ν_{88}, was calculated at (1417 ± 3) cm^{-1} (average ± range, as shown in Table 1S) and measured at (1418 ± 4) cm^{-1} and includes contributions from all bonds. Despite the generally weak IR and Raman intensities found for ν_{88}, it is a very well predicted mode, with rms values of 0−2 cm^{-1}. Another example of a mode with such good correspondence between the measured and theoretical spectra is ν_{89}, a terthiophene C═C symmetric stretch calculated and found experimentally at (1432 ± 1) cm^{-1}. As predicted, weak to medium IR and Raman intensities were measured for this mode. The exceptionally close similarity between both the average frequency and range values for these two modes indicates not only that the calculations predict the modes very accurately but also that they predict their highly conserved nature.

The modes associated with the terthiophene unit have significantly smaller calculated frequency ranges than those localized on the phenyl ring. This is also found in the experimental data. For example, one of the terthiophene C═C asymmetric stretches, ν_{95}, was calculated at (1548 ± 0) cm^{-1} and measured at (1558 ± 3) cm^{-1}. In contrast, the phenyl asymmetric stretching mode ν_{87} was calculated at (1415 ± 21) cm^{-1} and observed at (1422 ± 26) cm^{-1}. This large variation is due to the differing nature of the R group throughout the series of molecules. Since R is directly connected to the phenyl group, it is able to influence the frequency of the phenyl-based modes, and thus, these modes occur at more widely varying frequencies. However, the terthiophene unit is spatially too distant for R to have any major effect on its modes; hence, these frequencies vary considerably less. There appears to be no trends

TABLE 2: Correlated Modes and Calculated (B3LYP/6-31G(d)) and Experimental Vibrational Frequencies and Relative IR and Raman Intensities for Each R-pet Molecule

$\tilde{\nu}$/cm^{-1} (IR,R int)[a]																									
NMe_2-pet				NH_2-pet				MeO-pet				H-pet													
calc		expt		calc		expt		calc		expt		calc		expt		ν[b]	assignment								
961	(5,7)	959	(33,29)	962	(12,6)	955	(34,5)	962	(5,7)	956	(sh,sh)	966	(32,9)	960	(100,0)	63	γ(CH)$_{ethene}$								
971	(6,2)	989	(6,4)	971	(10,2)	990	(1,4)	972	(5,2)	964	(22,21)	972	(66,2)			64	γ(CH)$_{ethene}$								
985	(0,0)	976	(8,0)	988	(0,0)			988	(0,0)	992	(0,4)	975	(3,2)	982	(sh,0)	65	ν(CC)$_{phenyl\ skeletal}$								
1038	(1,1)	1049	(7,3)	1038	(3,2)	1049	(11,3)	1038	(1,2)	1052	(sh,3)	1039	(23,3)	1049	(22,4)	66	δ(CH)$_{terthiophene}$								
1038	(2,2)			1039	(3,1)			1039	(2,1)			1038	(13,1)			67	δ(CH)$_{terthiophene}$								
1070	(0,1)	1080	(5,3)	1071	(1,1)	1080	(10,4)	1071	(1,1)	1081	(6,8)	1071	(6,1)	1080	(16,5)	68	δ(CH)$_{terthiophene}$								
1071	(0,0)			1071	(1,0)			1071	(0,0)			1072	(4,1)			69	δ(CH)$_{terthiophene}$								
1119	(0,0)			1120	(3,0)	1126	(4,0)	1100	(2,0)	1110	(8,0)					71	δ(CH)$_{phenyl}$								
1179	(20,20)	1187	(49,44)	1167	(40,16)	1178	(61,22)	1163	(23,15)	1175	(51,28)	1168	(2,6)	1178	(sh,sh)	72	δ(CH)$_{phenyl}$								
1172	(4,8)			1172	(9,6)	1190	(sh,10)	1172	(4,6)	1183	(sh,sh)	1173	(31,8)			73	ν(C−S) and δ(CH)$_{terthiophene}$								
1175	(7,7)			1176	(12,3)			1176	(6,3)	1189	(sh,sh)	1177	(68,4)			74	ν(C−S) and δ(CH)$_{terthiophene}$								
				1202	(2,11)	1212	(3,9)	1198	(0,11)	1209	(0,11)	1195	(6,14)	1209	(13,13)	75	δ(CH)$_{phenyl}$ and δ(CH)$_{ethene}$								
1207	(0,1)			1207	(1,2)			1207	(0,2)			1207	(5,3)			76	ν(C−S) and δ(CH)$_{terthiophene}$								
1214	(0,9)	1219	(sh,sh)	1213	(0,6)	1231	(7,4)	1214	(0,6)	1229	(0,sh)	1214	(5,6)	1231	(26,6)	77	δ(CH)$_{terthiophene}$ and δ(CH)$_{ethene}$								
1223	(2,1)	1242	(11,9)	1222	(3,1)	1242	(7,5)	1222	(2,1)	1238	(0,11)	1223	(11,2)	1244	(26,7)	78	δ(CH)$_{terthiophene}$								
1272	(3,14)	1281	(8,16)	1266	(19,13)	1274	(33,16)	1270	(16,15)	1277	(28,5)	1264	(10,9)	1273	(11,10)	79	δ(CH)$_{delocalized}$								
				1299	(0,9)	1310	(0,10)	1295	(2,3)	1304	(17,0)	1303	(20,8)	1301	(7,0)	80	δ(CH)$_{delocalized}$								
1302	(0,13)	1301	(2,19)	1318	(6,5)	1330	(5,8)	1308	(10,5)	1311	(sh,16)	1315	(4,3)	1309	(6,8)	81	δ(CH)$_{delocalized}$								
1324	(5,9)	1333	(sh,8)	1323	(1,5)			1324	(5,10)			1325	(2,7)	1332	(1,8)	82	δ(CH)$_{ethene}$ and δ(CH)$_{terthiophene}$								
1340	(3,1)			1340	(1,1)	1348	(0,5)	1339	(2,1)	1351	(2,6)	1339	(4,1)	1352	(6,6)	85	δ(CH)$_{ethene}$								
1372	(0,13)	1384	(0,19)	1372	(1,14)	1384	(0,21)	1372	(0,13)	1383	(3,20)	1373	(3,14)	1386	(12,22)	86	ν(C−C)$_{terthiophene}$								
1428	(1,3)			1429	(1,7)	1429	(0,sh)	1408	(3,1)	1415	(0,7)	1436	(15,25)	1448	(28,38)	87	ν_a(C=C)$_{phenyl}$								
1417	(6,1)	1417	(9,0)	1415	(15,1)	1416	(17,11)	1420	(3,4)	1422	(sh,16)	1416	(42,2)	1417	(28,15)	88	$\nu_{delocalized}$								
1433	(2,4)	1432	(8,13)	1433	(5,5)	1433	(10,18)	1432	(2,4)	1432	(sh,15)	1432	(22,4)	1432	(18,15)	89	ν_s(C=C)$_{terthiophene}$								
1446	(0,86)	1459	(7,82)	1446	(0,100)	1460	(9,100)	1446	(0,100)	1458	(sh,100)	1448	(5,100)	1462	(16,100)	90	ν_s(C=C)$_{terthiophene}$								
1514	(56,4)	1522	(96,0)	1507	(66,2)	1515	(100,0)	1505	(38,2)	1513	(90,0)	1484	(32,4)	1494	(27,sh)	91	ν_s(C=C)$_{phenyl}$								
1500	(4,6)	1502	(8,8)	1500	(9,9)	1501	(16,9)	1499	(6,9)	1500	(sh,8)	1501	(100,7)	1503	(40,9)	92	ν_a(C=C)$_{terthiophene}$								
1523	(12,23)	1530	(sh,41)	1523	(11,27)	1525	(15,49)	1523	(3,27)	1528	(sh,64)	1524	(5,31)	1525	(7,50)	93	ν_a(C=C)$_{terthiophene}$								
1539	(2,5)	1551	(0,sh)	1557	(3,5)	1572	(10,sh)	1556	(2,3)	1576	(7,21)	1568	(4,5)	1576	(8,12)	94	ν_a(C=C)$_{phenyl}$								
1548	(3,21)	1558	(12,27)	1548	(4,23)	1560	(14,25)	1548	(2,22)	1558	(2,26)	1548	(0,26)	1556	(3,38)	95	ν_a(C=C)$_{terthiophene}$								
1600	(99,100)	1603	(100,100)	1600	(100,68)	1603	(91,67)	1598	(42,70)	1605	(44,44)	1593	(36,40)	1598	(37,35)	96	ν_s(C=C)$_{phenyl}$ and ν(C=C)$_{ethene}$								
1624	(3,36)	1622	(0,95)	1630	(65,6)	1621	(sh,sh)	1626	(2,45)	1626	(3,97)	1626	(2,59)	1628	(6,62)	98	ν(C=C)$_{ethene}$								

$\tilde{\nu}$/cm^{-1} (IR,R int)													
pyr-et				CN-pet				NO_2-pet					
calc		expt		calc		expt		calc		expt		ν	assignment
971	(7,1)			964	(12,5)	950	(24,3)	966	(2,5)	956	(12,9)	63	γ(CH)$_{ethene}$
974	(10,1)			973	(8,1)	966	(34,10)	973	(2,1)	967	(15,4)	64	γ(CH)$_{ethene}$
				995	(0,1)	994	(5,3)	990	(0,3)	1009	(0,4)	65	ν(CC)$_{phenyl\ skeletal}$
1039	(2,0)	1051	(15,4)	1039	(3,1)	1048	(11,2)	1039	(1,1)	1049	(4,2)	66	δ(CH)$_{terthiophene}$
1039	(4,3)			1039	(5,2)			1039	(1,2)			67	δ(CH)$_{terthiophene}$
1071	(1,1)	1081	(12,4)	1072	(1,1)	1080	(7,3)	1072	(0,1)	1079	(3,4)	68	δ(CH)$_{terthiophene}$
1072	(1,0)			1072	(0,0)			1072	(0,0)			69	δ(CH)$_{terthiophene}$
1080	(0,0)			1103	(1,0)	1109	(4,1)	1095	(1,0)			71	δ(CH)$_{phenyl}$
				1161	(15,33)	1174	(34,30)	1169	(1,3)			72	δ(CH)$_{phenyl}$
1173	(7,5)	1175	(9,sh)	1173	(9,4)	1188	(18,8)	1173	(5,16)	1185	(9,29)	73	ν(C−S) and δ(CH)$_{terthiophene}$
1177	(9,3)	1189	(10,8)	1178	(10,3)			1178	(2,3)			74	ν(C−S) and δ(CH)$_{terthiophene}$
1192	(2,12)	1205	(2,11)	1200	(2,14)	1213	(sh,10)	1197	(2,25)	1211	(0,15)	75	δ(CH)$_{phenyl}$ and δ(CH)$_{ethene}$
1207	(1,1)			1207	(2,3)			1207	(1,5)			76	ν(C−S) and δ(CH)$_{terthiophene}$
1214	(1,6)	1233	(7,sh)	1215	(3,5)	1231	(13,4)	1214	(1,7)	1233	(5,0)	77	δ(CH)$_{terthiophene}$ and δ(CH)$_{ethene}$
1224	(2,2)	1242	(14,16)	1224	(2,1)	1242	(14,5)	1223	(1,1)	1242	(5,9)	78	δ(CH)$_{terthiophene}$
1285	(5,5)	1291	(14,10)	1265	(4,10)	1273	(3,7)	1268	(3,15)	1277	(3,15)	79	δ(CH)$_{delocalized}$
				1304	(16,9)	1310	(12,8)	1290	(3,6)	1306	(7,sh)	80	δ(CH)$_{delocalized}$
1307	(5,7)	1312	(6,10)	1319	(1,6)	1324	(0,9)	1311	(13,28)	1322	(sh,sh)	81	δ(CH)$_{delocalized}$
1327	(1,4)	1337	(3,9)	1324	(1,6)	1336	(2,3)	1321	(0,1)			82	δ(CH)$_{ethene}$ and δ(CH)$_{terthiophene}$
1340	(1,1)	1352	(6,sh)	1340	(3,1)	1349	(sh,3)	1342	(1,1)			85	δ(CH)$_{ethene}$
1374	(3,11)	1388	(8,17)	1374	(4,12)	1387	(6,14)	1375	(1,12)	1387	(3,16)	86	ν(C−C)$_{terthiophene}$
1403	(6,1)	1417	(40,12)	1402	(2,2)	1410	(16,0)	1401	(0,2)	1410	(3,4)	87	ν_a(C=C)$_{phenyl}$
1417	(9,3)			1418	(8,3)	1417	(16,8)	1418	(2,4)	1419	(4,7)	88	$\nu_{delocalized}$
1432	(3,4)	1432	(sh,11)	1432	(4,4)	1431	(8,8)	1432	(1,5)	1431	(3,8)	89	ν_s(C=C)$_{terthiophene}$
1446	(4,100)	1461	(15,100)	1446	(6,87)	1461	(10,50)	1446	(2,95)	1461	(3,45)	90	ν_s(C=C)$_{terthiophene}$
1482	(4,2)			1492	(9,4)	1499	(sh,5)	1480	(1,2)			91	ν_s(C=C)$_{phenyl}$
1501	(14,7)	1503	(15,6)	1502	(18,5)	1509	(24,0)	1501	(3,8)	1503	(0,9)	92	ν_a(C=C)$_{terthiophene}$
1524	(0,26)	1527	(4,59)	1524	(0,24)	1528	(4,36)	1524	(0,29)	1527	(0,33)	93	ν_a(C=C)$_{terthiophene}$
1537	(7,5)	1548	(20,sh)	1535	(1,7)	1544	(sh,sh)	1540	(13,4)	1518	(52,0)	94	ν_a(C=C)$_{phenyl}$
1548	(2,22)	1559	(sh,25)	1548	(2,21)	1559	(3,20)	1548	(1,25)	1555	(0,16)	95	ν_a(C=C)$_{terthiophene}$
1583	(100,25)	1593	(100,26)	1591	(100,100)	1602	(100,100)	1582	(33,100)	1591	(35,100)	96	ν_s(C=C)$_{phenyl}$ and ν(C=C)$_{ethene}$
1624	(11,51)	1625	(21,72)	1623	(9,43)	1629	(15,60)	1620	(5,62)	1626	(9,100)	98	ν(C=C)$_{ethene}$

[a] Relative IR and Raman intensities, normalized such that the most intense band in the reported spectral region is 100. sh = shoulder. [b] Mode number.

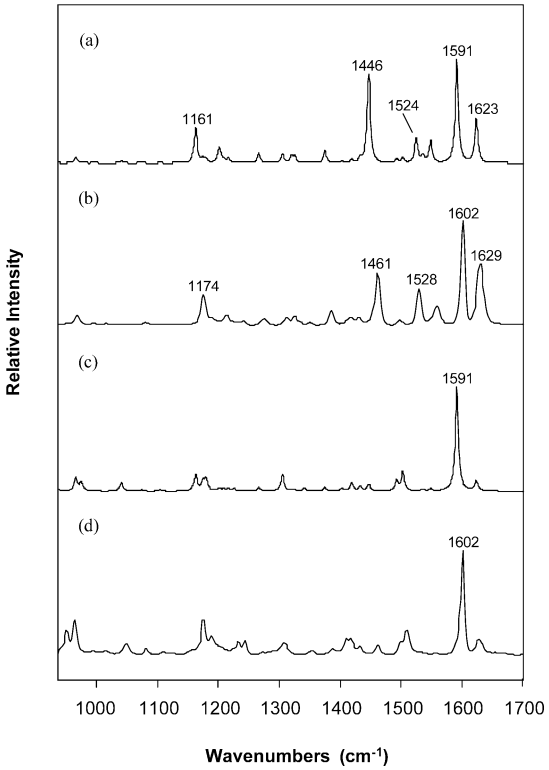

Figure 3. Comparison of the theoretical B3LYP/6-31G(d) Raman (a), experimental Raman (b), theoretical B3LYP/6-31G(d) IR (c), and experimental IR (d) spectra of CN-pet. Raman spectra were measured using 1064 nm excitation and were calculated using the same wavelength. Numbers denote the frequency of the bands in wavenumbers (cm^{-1}).

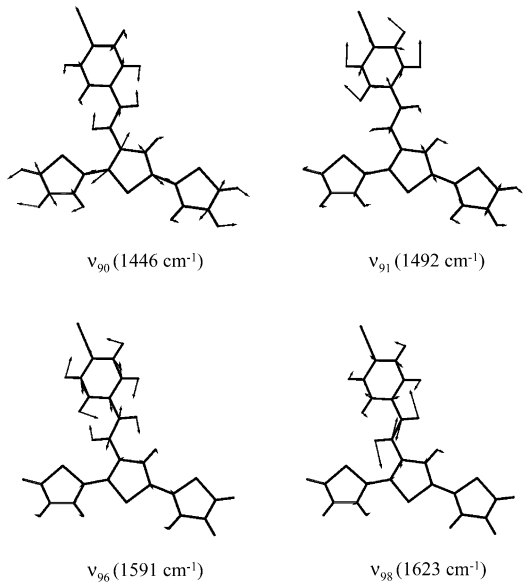

Figure 4. Eigenvectors illustrating selected vibrational modes of CN-pet that are generally intense across the R-pet series, calculated using the B3LYP/6-31G(d) method. Calculated vibrational frequencies are shown in brackets.

in the variation of the phenyl-based mode frequencies with respect to the electron withdrawing capability of the R group.

The Raman spectra of oligothiophenes are, in general, relatively simple. The four most intense bands are often denoted as lines A, B, C, and D.[53] Line A exhibits frequency and intensity dispersions with increasing chain length. For example, line A of the α,α′-dimethyl end-capped oligothiophene series displays a significant frequency downshift from the terthiophene to the quaterthiophene: 1546, 1533, and 1525 cm^{-1}.[54] This line corresponds to a totally symmetric ν_{as}(C═C) mode, where the majority of the amplitude is on the end rings.[53,55] Line B is the strongest band in the Raman spectrum, shows little to no frequency dispersion,[56] and belongs to a totally symmetric ν_s(C═C) mode. For unsubstituted oligothiophenes, line B appears at approximately 1460 cm^{-1}. Line C is only observed in end-capped oligothiophenes and therefore is not applicable to the R-pet system. Line D is a symmetric C−H bending mode of the β hydrogens. It usually appears as a medium intensity band at 1050−1080 cm^{-1}.

The Raman spectra of R-pet are considerably more complicated than those of unsubstituted and end-capped oligothiophenes due to the presence of the large substituent, which contributes numerous phenyl- and ethenyl-based modes. However, lines A and B are still clearly observed, despite the fact that the calculated modes are not totally symmetric. The mode ν_{93} at (1527 ± 3) cm^{-1} has been identified as line A. Line B is obviously ν_{90} at (1460 ± 2) cm^{-1}, since it is usually the most intense Raman band. This is very similar to the frequency of line B in unsubstituted terthiophene, 1463 cm^{-1}.[31] Line D is observed at (1050 ± 2) cm^{-1} but in contrast to the cases of other oligothiophenes is of very weak intensity.

The use of line A's frequency dispersion with chain length to assess effective conjugation length has been suggested, although this mode's pronounced end group character may limit this application.[53] The position of line A for R-pet, (1527 ± 3) cm^{-1}, is comparable to its position in the pentamers of both α,α′-dimethyl[54] and α,α′-diethyl[57] end-capped oligothiophenes (1525 and 1527 cm^{-1}, respectively). This may suggest an effective conjugation length in R-pet of approximately five thiophene units. This in turn implies that the electronically active phenyl ethenyl substituent is significantly increasing the effective conjugation length of the base terthiophene unit. This result can be tested by comparison of another of the ν_{as}(C═C) modes with the corresponding mode in the α,α′-dimethyl end-capped series.[53] The R-pet mode ν_{92} occurs at (1503 ± 6) cm^{-1} and, taking into account the larger frequency range observed for this mode, is close to the corresponding modes in the pentamer (1508 cm^{-1}) and hexamer (1503 cm^{-1}), thus substantiating the above result. The wavenumber of line A for R-pet does not shift appreciably across the series, suggesting that the R group does not influence the effective conjugation length.

The effective conjugation coordinate (ECC) theory was developed to account for some of the features observed in the Raman spectra of conjugated oligomers.[31,58,59] In such systems there exists a particular vibrational coordinate, known as $\mathscr{R}$, that describes the path the π electrons follow during the transition between the ground electronic state and the first electronic excited state. This vibrational coordinate is unique for each molecular system but always belongs to a totally symmetric mode of the system being considered. For simple oligothiophenes, this is an in-phase oscillation of the alternating C═C and C−C bonds of the π-conjugated backbone and therefore mimics the geometrical modifications which occur during the $\pi-\pi^*$ electronic transition or ionization (that is, the evolution of the π-conjugated backbone from a benzenoid to a quinoid structure). It is well-known that the strong bands present in a Raman spectrum of a conjugated oligomer originate from totally symmetric modes that possess a substantial contribution from $\mathscr{R}$.[56] The mode for which the Raman intensity is greatest contains the largest content of $\mathscr{R}$ and is called the $\mathscr{R}$ or ECC mode. Another characteristic of this ECC mode is that it is strongly coupled to π-conjugation. A key parameter in ECC

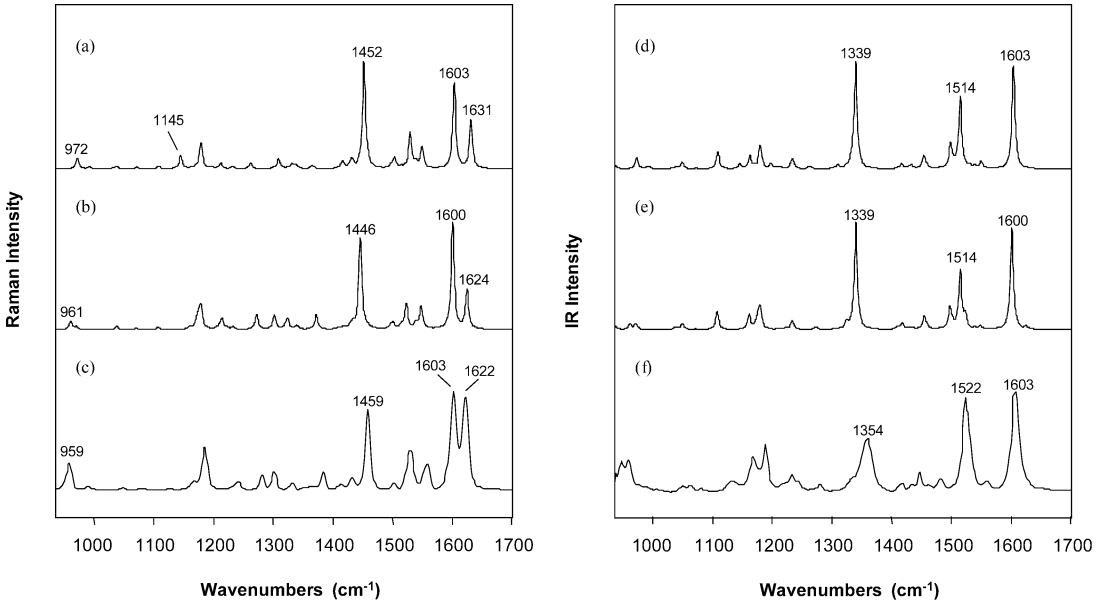

Figure 5. Comparison of the theoretical B3LYP/6-31G(d) Raman spectra of conformers 1 (a) and 2 (b) of NMe_2-pet with the experimental Raman spectrum (c). Also compared are the theoretical B3LYP/6-31G(d) IR spectra of conformers 1 (d) and 2 (e) of NMe_2-pet with the experimental IR spectrum (f).

theory is the effective force constant associated with $\mathscr{R}$ (referred to as $F_{\mathscr{R}}$), which is linearly related to the HOMO−LUMO energy difference (E_g). A longer conjugation length results in a smaller E_g and $F_{\mathscr{R}}$ and, therefore, causes, under the terms of ECC theory, a decrease in the frequency and Raman intensity of the ECC mode.[31] Although this has been observed in other oligomers such as oligofurans and oligopyrroles, the ECC mode of oligothiophenes (line B, $\sim$1460 cm^{-1}) shows little to no frequency dispersion with increasing chain length.[56] This is thought to be due to a significant confinement potential within the individual rings that opposes delocalization of the π electrons along the molecular chain.

The application of ECC theory to R-pet is not as straightforward as it is for simple oligothiophenes. This is primarily due to the asymmetry of the system, which negates completely symmetrical normal modes. The R-pet mode closest in nature to the conventional oligothiophene ECC mode is ν_{90} at (1460 $\pm$ 2) cm^{-1}. As previously stated, this mode has been identified as line B and is usually the strongest Raman band, as expected from ECC theory. Line B has been recognized as the ECC mode in various other oligothiophenes.[53,57,60,61] In contrast, however, the most intense Raman band for NO_2-pet, CN-pet, and NMe_2-pet is ν_{96} (Figure 4), a symmetrical mode localized solely on the phenyl ethenyl group. This observation may suggest that the ECC mode has switched to this substituent-based mode for those molecules in the R-pet series with the strongest electron withdrawing or donating R groups, whereas those molecules with an R group of intermediate electronic influence have a primarily thiophene-based ECC mode. Therefore, the probable nature of the frontier molecular orbitals involved in each case can be derived, since the ECC mode reflects the transition to the first electronic excited state. For pyr-et, H-pet, MeO-pet, and NH_2-pet, both the HOMO and LUMO should contain contributions from the terthiophene unit and the transition between the two should bear some of the characteristics of a normal oligothiophene $\pi-\pi^*$ transition. NO_2-pet, CN-pet, and NMe_2-pet, however, should contain frontier MOs in which a significant portion of the orbital density is localized on the phenyl ethenyl substituent. The calculated molecular orbitals (Figure 7, discussed in section III.e) support these predictions. NO_2-pet's and CN-pet's LUMOs and NMe_2-pet's HOMO are localized primarily on the substituent. Conversely, the other molecules have both MOs based on the terthiophene (H-pet in particular and NH_2-pet to a lesser extent).

III.d. Conformational Dependence of Spectra. It is expected that different R-pet conformations will have different vibrational spectra, in terms of both intensity and frequency. A change in conformation alters the dipole moment: conformer 1 of NO_2-pet, for example, was calculated to have a dipole moment of 6.34 D, whereas conformer 2 has one of 7.10 D. The dipole moment vectors for both of these conformers are positioned along the phenyl ethenyl substituent and point toward the terthiophene unit, but the directions differ by approximately 10°. Because the transition moment integral is a function of the dipole moment, it therefore follows that the intensities of vibrational spectra will be dependent upon conformation. Frequencies are also reliant upon geometry. In this class of molecules, a more twisted structure has reduced p orbital overlap, which alters the force constants and thus shifts the resulting frequencies.[31] The vibrational spectra of bithiophene show only a minor conformational dependence.[17,62] Anti and anti-gauche geometries produce virtually identical spectra, as do syn and syn-gauche. Syn and anti calculated frequencies for the same mode can differ by up to 40 cm^{-1} in the 900−1700 cm^{-1} region, while the perpendicular conformation shows intensity enhancements and red-shifts of particular modes. The appearance of more than one geometry in measured spectra has been observed in other work accomplished on bithiophene[17] and terthiophene.[31]

Vibrational spectra were calculated for conformers 1 and 2 (as described in the geometry section) of NMe_2-pet. These spectra are shown in Figure 5 and compared to the measured spectra. In general, the spectra for the two conformations of NMe_2-pet are very similar and differ by only slight alterations in frequency and intensity. The experimental vibrational spectra indicate that both NMe_2-pet conformations are present. For example, the broad band measured at 1522 cm^{-1} in the IR spectrum has a significant shoulder at 1526 cm^{-1}, both of which have been assigned to the ν_{91} mode. The splitting of this calculated band suggests the presence of at least two different conformations.

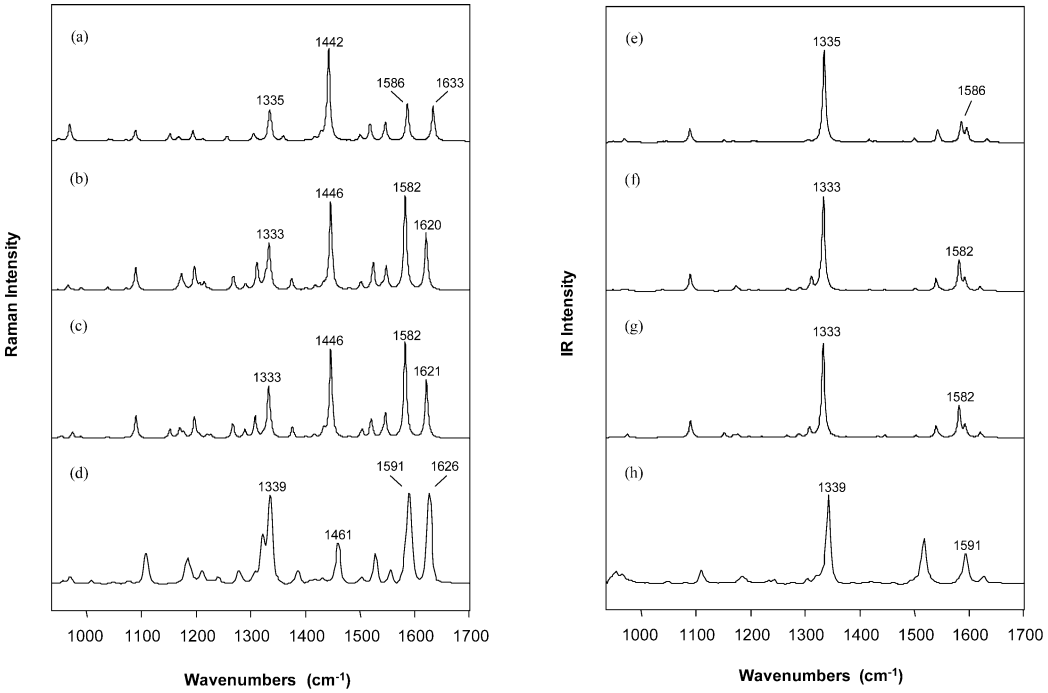

Figure 6. Comparison of the theoretical B3LYP/6-31G(d) Raman spectra of conformers 1 (a), 2 (b), and 3 (c) of NO_2-pet with the experimental Raman spectrum (d). Also compared are the theoretical B3LYP/6-31G(d) IR spectra of conformers 1 (e), 2 (f), and 3 (g) of NO_2-pet with the experimental IR spectrum (h).

Evidence in favor of conformer 1 includes the two Raman bands in the 1410−1432 cm^{-1} region. While the calculated Raman spectrum of conformer 1 displays two well-defined peaks at 1416 (ν_{88}) and 1432 cm^{-1} (ν_{89}), that of conformer 2 does not. Two peaks are clearly visible in the experimental spectrum of conformer 1 at 1412 and 1432 cm^{-1}. In addition, the relative intensities of the ν_{93} and ν_{95} modes in the measured Raman spectrum more closely match the intensities of the corresponding peaks in the calculated spectrum of conformer 1. However, there is also evidence that conformer 2 of NMe_2-pet contributes to the experimental spectra. The intensities of the peaks in the 1200−1400 cm^{-1} region of the experimental Raman spectrum are appreciably closer to that predicted for this conformer, particularly for the modes ν_{79} and ν_{86} (1281 and 1384 cm^{-1}). Frequencies correlate more accurately with conformer 2 in this specific region as well. For instance, the band at 1281 cm^{-1} was predicted to occur at 1272 cm^{-1} for conformer 2 and 1262 cm^{-1} for conformer 1. In addition, one band calculated for conformer 1 at 972 cm^{-1} (ν_{63}) corresponds to a band calculated at 961 cm^{-1} for conformer 2. The calculated frequencies are outside the resolution of 4 cm^{-1}, and conformer 2 is closer to the measured peak at 959 cm^{-1}.

Three different conformations were considered for NO_2-pet: conformers 1−3. This was done in order to assess the differences that the syn-gauche geometry produces in the calculated vibrational spectra and whether this particular conformation can be observed experimentally. The measured and theoretical spectra are displayed in Figure 6. When the calculated spectra for each conformer of NO_2-pet are compared, it can be observed that conformers 2 and 3 present very similar spectra that contain only subtle differences. For example, conformer 3 has a band of weak intensity at 1152 cm^{-1} that has a counterpart in neither the spectra of conformer 2 nor experiment. However, the spectra of conformers 2 and 3 are noticeably different from that of conformer 1. This is particularly evident in the Raman spectra. An example of this is ν_{96}, which was calculated at 1582 cm^{-1} for conformers 2 and 3 and 1586 cm^{-1} for 1. Although the frequencies match well, the latter's Raman intensity is significantly less, by 60%. The assigned measured band has a relative Raman intensity of 100, which matches that of conformers 2 and 3 (100) and is significantly different from that of conformer 1 (40). There are also large frequency changes between the two different geometries. For instance, conformer 2 and 3's ν_{79} mode at 1268 cm^{-1} corresponds to 1256 cm^{-1} in conformer 1, and a weak band calculated at 1376 cm^{-1} (ν_{86}) for conformers 2 and 3 is reproduced at 1359 cm^{-1} for conformer 1. In both of these cases, conformers 2 and 3 match the experimental frequencies (1277 and 1387 cm^{-1}, respectively) more closely than conformer 1 does.

The three NO_2-pet structures have comparable rms values (10−11 cm^{-1}). Despite this, the higher intensities of conformer 2 and 3's spectra more closely match those of both the experimental IR and Raman spectra; thus, it seems probable that conformers 2 and 3 are preferred over conformer 1. However, because there are only slight differences between the spectra of conformers 2 and 3, it is difficult to discern whether either of these two geometries is favored experimentally.

The conclusions reached concerning the various geometries of NO_2-pet and NMe_2-pet are consistent with the previous results from the conformation section. NO_2-pet has a larger energy difference between conformers 1 and 2 than NMe_2-pet; hence, it was considered more likely that the latter molecule would exhibit more than one conformation. This is not inconsistent with the experimental IR and Raman spectra: NMe_2-pet shows evidence of the two conformations, whereas NO_2-pet demonstrates clear support for a preference of conformers 2 and 3 over conformer 1. The probable appearance of both conformers 2 and 3 in the experimental spectra of NO_2-pet reflects the previous finding that the anti-gauche and syn-gauche geometries are separated by only a small energy difference and that both would therefore be expected to appear experimentally.

III.e. Molecular Orbitals and Electronic Absorption Spectra. It was concluded in the previous section that the calculated vibrational spectra match the experimental spectra;

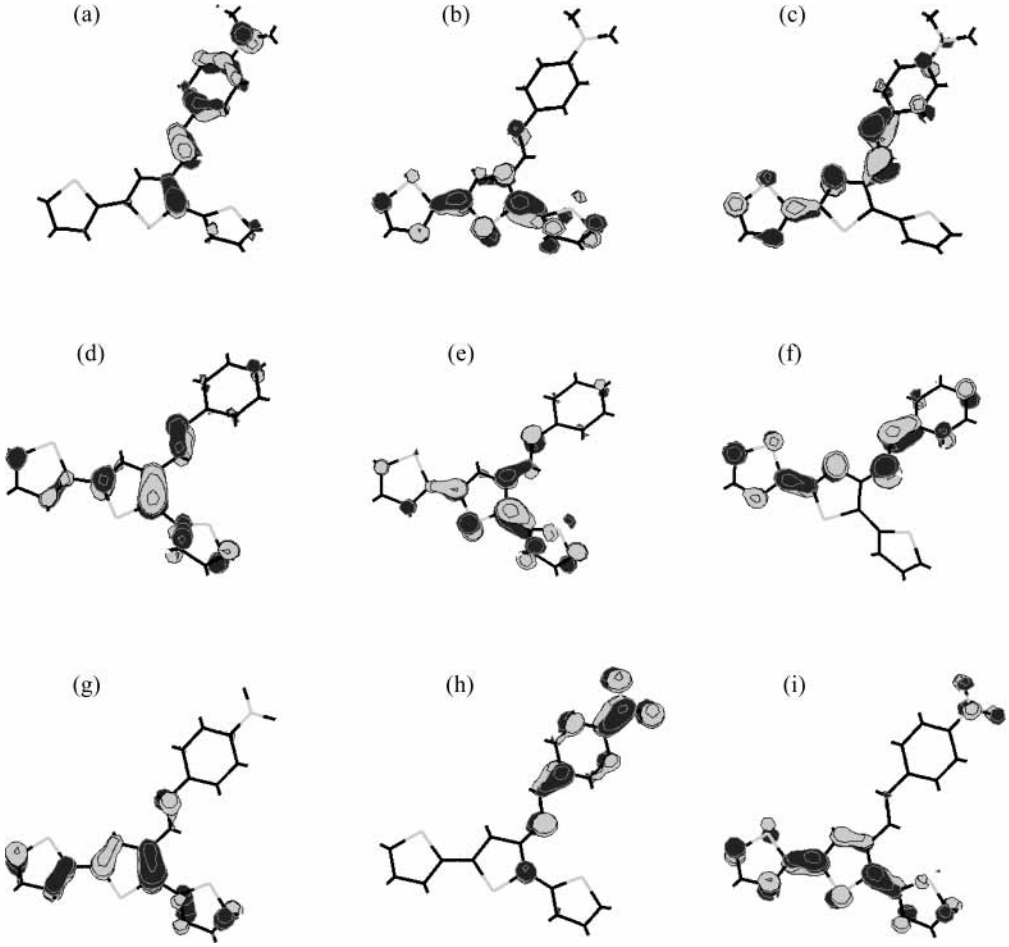

Figure 7. (a) HOMO, (b) LUMO, and (c) LUMO+1 of NMe_2-pet; (d) HOMO, (e) LUMO, and (f) LUMO+1 of H-pet; and (g) HOMO, (h) LUMO, and (i) LUMO+1 of NO_2-pet, as calculated using the B3LYP/6-31G(d) method.

thus, it can be assumed that the calculated geometries are reliable models of the true structures. Therefore, the calculated molecular orbitals (MOs) provide a reasonable first approximation of the electronic distribution in the R-pet molecules. The energies, occupancies, and positions of the MOs were calculated using the B3LYP/6-31G(d) method for each molecule. The HOMOs, LUMOs, and LUMO+1's of NO_2-pet, H-pet, and NMe_2-pet are shown in Figure 7. As expected for a conjugated system, the HOMOs have the same phase across the double bonds, and the LUMOs have the same phase across the single bonds. This result has been seen in other work[38] and is general for polyenic chains.

Various trends are observed in the MOs across the R-pet series. The molecules with strong electron donating R groups, such as NMe_2-pet, have HOMOs with the greatest electron density on the functionalized phenyl ethenyl unit, whereas the molecules with strong electron withdrawing R groups (NO_2-pet, for example) have the largest electron density situated on the terthiophene unit. The LUMOs exhibit the opposite trend: NMe_2-pet has these orbitals on the terthiophene while they are mostly located on the functionalized phenyl ethenyl unit for NO_2-pet. The molecules in between show a gradual transition between these two situations. This trend is intuitive; a molecule such as NO_2-pet must have empty orbitals localized on the R group in order to act as an electron acceptor, while NMe_2-pet must have full orbitals on the NMe_2 functionality in order to donate electrons.

In order for efficient conductivity to occur, charge separation of the excitons that form upon photoirradiation is required. This would be facilitated by the spatial separation of the HOMO and LUMO that is observed in the strongly electron withdrawing and donating molecules, since the first excited state would involve charge-transfer characteristics.[63] In addition, NO_2-pet and the other electron accepting molecules should have an advantage over the electron donators in that the orientation of the frontier MOs is such that the tendency for a polythiophene backbone to preferentially carry holes[6,64,65] is promoted.

The positions of the calculated MOs (Figure 7) would be expected to have implications in the electronic absorption spectra. In NO_2-pet and NMe_2-pet there is little orbital overlap between the HOMO and the LUMO; thus, this electronic transition is expected to have a weak absorbance. Conversely, there appears to be significant overlap between the HOMO and LUMO+1, and therefore, this transition is likely to be much more intense. H-pet, in contrast, has substantial overlap between the two frontier orbitals, and consequently, the HOMO−LUMO transition should be more intense than those for the other compounds. The measured electronic absorption spectra (Figure 8) follow these qualitative predictions. In general, the R-pet series show a maximum absorption peak at 310−355 nm and a shoulder at 360−415 nm. These peaks correspond to the HOMO−LUMO+1 and HOMO−LUMO transitions, respectively. In all cases, the HOMO−LUMO+1 transition is the strongest. The HOMO−LUMO transition is considerably less intense and appears as a weak shoulder that is most pronounced in H-pet, as expected.

Examination of the calculated molecular orbital energies shows that H-pet and pyr-et have the largest HOMO−LUMO and HOMO−LUMO+1 energy gaps, whereas NO_2-pet and

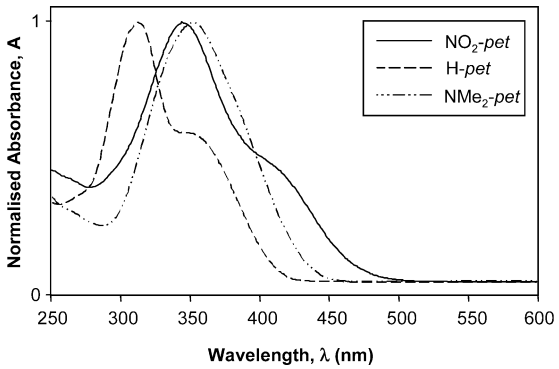

Figure 8. Electronic absorption spectra of NO_2-pet, H-pet, and NMe_2-pet, as measured in CH_2Cl_2. The intensities of each maximum absorption peak have been normalized to 1.

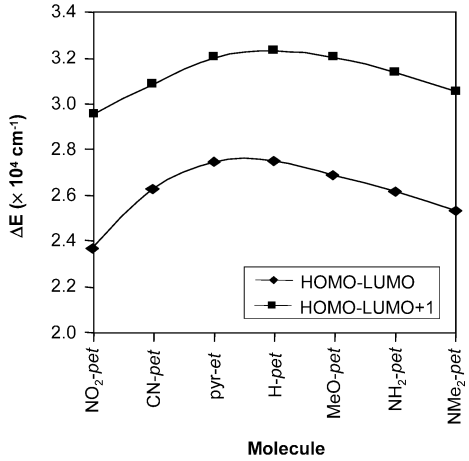

Figure 9. Energy differences (ΔE) between the HOMO and LUMO and the HOMO and LUMO+1, as calculated using the B3LYP/6-31G(d) method.

NMe_2-pet have the smallest. When the order of the electron donating capacity is taken into account, these energy gaps follow an approximately parabolic relationship across the R-pet series (Figure 9). It is well-known that electron donating groups raise the HOMO while electron withdrawing groups lower the LUMO. Both of these effects result in a decreased HOMO−LUMO gap. The red-shift effect of the electron donating and withdrawing groups predicted from the calculated orbital energies is observed experimentally for these transitions, as shown in Figure 8. The maximum red-shift of 64 nm (4394 cm^{-1}) occurs from H-pet to NO_2-pet for the HOMO−LUMO transition (predicted to be 3887 cm^{-1}).

It can therefore be concluded that the experimental electronic absorption spectra qualitatively support the positions and trends in energies of the R-pet molecular orbitals. The molecular orbital energies can also be used as an approximate guide for predicting the wavelengths at which electronic transitions will occur. The energy differences between the appropriate orbitals were calculated and compared to the transition wavelengths in the experimental R-pet electronic absorption spectra (Table 2S). An extremely good correlation was not expected because the energy of a transition is not solely based on the energy difference between the two MOs (when an electron is promoted to form an excited state, that state also contributes to the energy of the transition: the energy of the higher orbital alters when it is occupied by the excited electron). There are a number of possibilities available in order to improve the theoretical predictions of electronic absorptions, including CIS[66] and time-dependent DFT[35,67] calculations. These methods will be applied to R-pet in the future.

IV. Conclusions

Conformational analyses of 3′-[1*E*-2-(4-R-phenyl)ethenyl]-2,2′:5′,2″-terthiophenes revealed three important dihedral angles, and the potential energy surfaces for each of these angles were calculated for three R-pet molecules using the HF/3-21G(d) method. Each dihedral angle possesses a different energy curve, but the effect of the R group is small. For each R-pet examined, ϕ_1 has a very small energy barrier between the syn-gauche and anti-gauche conformations, while ϕ_2 prefers the anti-gauche arrangement and the energy minimum of ϕ_3 is at 0°.

Using the B3LYP/6-31G(d) method, the calculated IR and Raman spectra of the R-pet series were determined and compared to the corresponding experimental spectra. The calculated vibrational spectra correlate favorably with the experimentally obtained spectra. The frequency rms values range from 7 to 10 cm^{-1} and, with a few exceptions, the intensities also agree reasonably well. Thus, it can be assumed that the calculated structures of the neutral molecules are reasonable models of the true structures. The types of vibrational modes were assessed, and it was concluded that the majority of R-pet's vibrational modes are conserved, both theoretically and experimentally. Lines A, B, and D in the Raman spectra were identified. The frequency of line A suggests an effective conjugation length that includes a significant contribution from the phenyl ethenyl substituent. ECC theory is not as applicable to R-pet as it is to other oligothiophene systems studied, due to R-pet's asymmetry. However, the ECC mode could still be recognized in the Raman spectra of each molecule. NO_2-pet, CN-pet, and NMe_2-pet possess a substituent-based ECC mode while the other molecules have a typical terthiophene-based ECC mode. This observation allowed the probable nature of the frontier orbitals in each case to be established.

From the conformational dependence of the vibrational spectra, it appears that there is more than one conformation present in the vibrational spectra of NMe_2-pet. The measured spectra of NO_2-pet show that conformers 2 and 3 appear to be favored over conformer 1. Syn-gauche and anti-gauche conformations cannot be differentiated accurately.

The features of the calculated molecular orbitals (their positions and the trends in the energy gaps) are supported by experimental electronic absorption spectra. Consideration of the calculated molecular orbitals shows that, for the strongly electron withdrawing or donating molecules, the first excited state should have charge-transfer features. Since this would aid charge separation of the photoinduced exciton, this may prove to be a favorable characteristic of R-pet.

Acknowledgment. The authors are grateful to the New Zealand Foundation of Science, Research and Technology for support.

Supporting Information Available: A figure showing fitted potential energy surfaces of the dihedral angles ϕ_2, ϕ_1, and ϕ_3 of NMe_2-pet, NO_2-pet, and H-pet calculated using the HF/3-21G(d) method (Figure 1S), and tables showing the mode descriptions and average calculated (B3LYP/6-31G(d)) and experimental frequencies (± range) for each conserved mode over all R-pet molecules (Table 1S), and the predicted transition wavelengths (from the molecular orbital energy differences) compared to the experimental transition wavelengths of R-pet (Table 2S). This material is available free of charge via the Internet at http://pubs.acs.org.

References and Notes

(1) Shirakawa, H.; Louis, E. J.; MacDiarmid, A. G.; Chiang, C. K.; Heeger, A. J. *J. Chem. Soc., Chem. Commun.* **1977**, *16*, 578.

(2) (a) Katz, H. E. *J. Mater. Chem.* **1997**, *7*, 369. (b) Horowitz, G. *Adv. Mater.* **1998**, *10* (5), 365.

(3) (a)Burroughes, J. H.; Bradley, D. D. C.; Brown, A. R.; Marks, R. N.; Mackay, K.; Friend, R. H.; Burns, P. L.; Holmes, A. B. *Nature* **1990**, *347*, 539. (b) Dai, L.; Winkler, B.; Dong, L.; Tong, L.; Mau, A. W. H. *Adv. Mater.* **2001**, *13*, 915.

(4) Pron, A.; Rannou, P. *Prog. Polym. Sci.* **2002**, *27*, 135.

(5) Gazotti, W. A.; Nogueira, A. F.; Girotto, E. M.; Micaroni, L.; Martini, M.; das Neves, S.; De Paoli, M.-A. In *Handbook of Advanced Electronic and Photonic Materials and Devices*; Nalwa, H. S., Ed.; Academic Press: San Diego, CA, 2001.

(6) Daminelli, G.; Widany, J.; Di Carlo, A.; Lugli, P. *J. Chem. Phys.* **2001**, *115* (10), 4919.

(7) Roncali, J. *Chem. Rev.* **1992**, *92*, 711.

(8) Shaheen, S. E.; Brabec, C. J.; Sariciftci, N. S.; Padinger, F.; Fromherz, T.; Hummelen, J. C. *Appl. Phys. Lett.* **2001**, *78* (6), 841.

(9) Casado, J.; Hernández, V.; Hotta, S.; López Navarrete, J. T. *J. Chem. Phys.* **1998**, *109* (23), 10419.

(10) Ehrendorfer, Ch.; Karpfen, A. *Vib. Spectrosc.* **1995**, *8*, 293.

(11) Cutler, C. A.; Burrell, A. K.; Collis, G. E.; Dastoor, P. C.; Officer, D. L.; Too, C. O.; Wallace, G. G. *Synth. Met.* **2001**, *123*, 225.

(12) Khetrapal, C. L.; Kunwar, A. C. *Mol. Phys.* **1974**, *28*, 441.

(13) Bucci, P.; Longeri, M.; Veracini, C. A.; Lunazzi, L. *J. Am. Chem. Soc.* **1974**, *96*, 1305.

(14) Samdal, S.; Samuelsen, E. J.; Volden, H. V. *Synth. Met.* **1993**, *59*, 259.

(15) Chadwick, J. E.; Kohler, B. E. *J. Phys. Chem.* **1994**, *98*, 3631.

(16) Visser, G. J.; Heeres, G. J.; Wolters, J.; Vos, A. *Acta Crystallogr.* **1968**, *B24*, 467.

(17) Millefiori, S.; Alparone, A.; Millefiori, A. *Heterocycl. Chem.* **2000**, *37*, 847.

(18) Ortí, E.; Viruela, P. M.; Sánchez-Marin, J.; Tomás, F. *J. Phys. Chem.* **1995**, *99*, 4955.

(19) Alemán, C.; Juliá, L. *J. Phys. Chem.* **1996**, *100*, 1524.

(20) Alemán, C.; Domingo, V. M.; Fajarí, L.; Juliá, L.; Karpfen, A. *J. Org. Chem.* **1998**, *63*, 1041.

(21) Karpfen, A.; Choi, C. H.; Kertesz, M. *J. Phys. Chem. A* **1997**, *101*, 7426.

(22) Viruela, P. M.; Viruela, R.; Ortí, E.; Brédas, J. L. *J. Am. Chem. Soc.* **1997**, *119*, 1360.

(23) DiCésare, N.; Belletête, M.; Marrano, C.; Leclerc, M.; Durocher, G. *J. Phys. Chem. A* **1998**, *102*, 5142.

(24) Ciofalo, M.; La Manna, G. *Chem. Phys. Lett.* **1996**, *263*, 73.

(25) Diaz-Quijada, G. A.; Weinberg, N.; Holdcroft, S.; Pinto, B. M. *J. Phys. Chem. A* **2002**, *106*, 1266.

(26) DiCésare, N.; Belletête, M.; Donat-Bouillud, A.; Leclerc, M.; Durocher, G. *Macromolecules* **1998**, *31*, 6289.

(27) Hernández, V.; López Navarrete, J. T. *J. Chem. Phys.* **1994**, *101* (2), 1369.

(28) Ramírez, F. J.; Hernández, V.; López Navarrete, J. T. *J. Comput. Chem.* **1994**, *15* (4), 405.

(29) López Navarrete, J. T.; Tian, B.; Zerbi, G. *Synth. Met.* **1990**, *38*, 299.

(30) El-Azhary, A. A.; Hilal, R. H. *Spectrochim. Acta A* **1997**, *53*, 1365.

(31) Zerbi, G.; Chierichetti, B.; Inganäs, O. *J. Chem. Phys.* **1991**, *94* (6), 4637.

(32) Louarn, G.; Buisson, J. P.; Lefrant, S.; Fichou, D. *J. Phys. Chem.* **1995**, *99*, 11399.

(33) Ehrendorfer, Ch.; Karpfen, A. *J. Phys. Chem.* **1995**, *99*, 5341.

(34) Degli Esposti, A.; Moze, O.; Taliani, C.; Tomkinson, J. T.; Zamboni, R.; Zerbetto, F. *J. Chem. Phys.* **1996**, *104* (24), 9704.

(35) Casado, J.; Miller, L. L.; Mann, K. R.; Pappenfus, T. M.; Hernández, V.; López Navarrete, J. T. *J. Phys. Chem. B* **2002**, *106*, 3597.

(36) Cuff, L.; Kertesz, M. *J. Chem. Phys.* **1997**, *106* (13), 5541.

(37) Casado, J.; Hernández, V.; Kanemitsu, Y.; López Navarrete, J. T. *J. Raman Spectrosc.* **2000**, *31*, 565.

(38) Casado, J.; Miller, L. L.; Mann, K. R.; Pappenfus, T. M.; Kanemitsu, Y.; Ortí, E.; Viruela, P. M.; Pou-Amérigo, R.; Hernández, V.; López Navarrete, J. T. *J. Phys. Chem. B* **2002**, *106*, 3872.

(39) Casado, J.; Maraver Puig, J. J.; Hernández, V.; Zotti, G.; López Navarrete, J. T. *J. Phys. Chem. A* **2000**, *104*, 10656.

(40) Collis, G. E.; Burrell, A. K.; Officer, D. L. *J. Org. Chem.*, submitted for publication.

(41) PC *SPARTAN Pro*, version 1.5; Wavefunction, Inc.: 18401 Von Karman Ave., Suite 370, Irvine, CA 92612, 1998.

(42) Frisch, M. J.; Trucks, G. W.; Schlegel, H. B.; Scuseria, G. E.; Robb, M. A.; Cheeseman, J. R.; Zakrzewski, V. G.; Montgomery, J. A., Jr.; Stratmann, R. E.; Burant, J. C.; Dapprich, S.; Millam, J. M.; Daniels, A. D.; Kudin, K. N.; Strain, M. C.; Farkas, O.; Tomasi, J.; Barone, V.; Cossi, M.; Cammi, R.; Mennucci, B.; Pomelli, C.; Adamo, C.; Clifford, S.; Ochterski, J.; Petersson, G. A.; Ayala, P. Y.; Cui, Q.; Morokuma, K.; Malick, D. K.; Rabuck, A. D.; Raghavachari, K.; Foresman, J. B.; Cioslowski, J.; Ortiz, J. V.; Baboul, A. G.; Stefanov, B. B.; Liu, G.; Liashenko, A.; Piskorz, P.; Komaromi, I.; Gomperts, R.; Martin, R. L.; Fox, D. J.; Keith, T.; Al-Laham, M. A.; Peng, C. Y.; Nanayakkara, A.; Gonzalez, C.; Challacombe, M.; Gill, P. M. W.; Johnson, B.; Chen, W.; Wong, M. W.; Andres, J. L.; Gonzalez, C.; Head-Gordon, M.; Replogle, E. S.; Pople, J. A. *Gaussian 98*, Revision A.7; Gaussian, Inc.: Pittsburgh, PA, 1998.

(43) (a) Flükiger, P. F. Thèse No 2561, Département de chimie physique, Université de Genève, Genève, 1992. (b) Portmann, S.; Lüthi, H. P. *Chimia* **2000**, *54*, 766.

(44) Schaftenaar, G.; Noordik, J. H. *J. Comput.-Aided Mol. Des.* **2000**, *14*, 123.

(45) Scott, A. P.; Radom, L. *J. Phys. Chem.* **1996**, *100* (41), 16502.

(46) Belletête, M.; Di Césare, N.; Leclerc, M.; Durocher, G. *THEOCHEM* **1997**, *391*, 85.

(47) Fichou, D.; Bachet, B.; Demanze, F.; Billy, I.; Horowitz, G.; Garnier, F. *Adv. Mater.* **1996**, *8* (6), 500.

(48) Antolini, L.; Horowitz, G.; Kouki, F.; Garnier, F. *Adv. Mater.* **1998**, *10* (5), 382.

(49) Horowitz, G.; Bachet, B.; Yassar, A.; Lang, P.; Demanze, F.; Fave, J.; Garnier, F. *Chem. Mater.* **1995**, *7* (7), 1337.

(50) Barbarella, G.; Zambianchi, M.; Antolini, L.; Ostoja, P.; Maccagnani, P.; Bongini, A.; Marseglia, E. A.; Tedesco, E.; Gigli, G.; Cingolani, R. *J. Am. Chem. Soc.* **1999**, *121*, 8920.

(51) Yassar, A.; Garnier, F.; Deloffre, F.; Horowitz, G.; Ricard, L. *Adv. Mater.* **1994**, *6*, 660.

(52) Chaloner, P. A.; Gunatunga, S. R.; Hitchcock, P. B. *J. Chem. Soc., Perkin Trans. 2* **1997**, *8*, 1597.

(53) Hernández, V.; Casado, J.; Kanemitsu, Y.; López Navarrete, J. T. *J. Chem. Phys.* **1999**, *110* (14), 6907.

(54) Hernández, V.; Casado, J.; Ramírez, F. J.; Zotti, G.; Hotta, S.; López Navarrete, J. T. *J. Chem. Phys.* **1996**, *104* (23), 9271.

(55) Negri, F.; Zgierski, M. Z. *J. Chem. Phys.* **1994**, *100* (4), 2571.

(56) Hernández, V.; Castiglioni, C.; Del Zoppo, M.; Zerbi, G. *Phys. Rev. B* **1994**, *50* (14), 9815.

(57) Casado, J.; Hotta, S.; Hernández, V.; López Navarrete, J. T. *J. Phys. Chem. A* **1999**, *103*, 816.

(58) Castiglioni, C.; Gussoni, M.; López Navarrete, J. T.; Zerbi, G. *Solid State Commun.* **1988**, *65*, 625.

(59) Zerbi, G.; Castiglioni, C.; López Navarrete, J. T.; Tian, B.; Gussoni, M. *Synth. Met.* **1989**, *28*, D359.

(60) Hernández, V.; Casado, J.; Effenberger, F.; López Navarrete, J. T. *J. Chem. Phys.* **2000**, *112* (11), 5105.

(61) Casado, J.; Katz, H. E.; Hernández, V.; López Navarrete, J. T. *J. Phys. Chem. B* **2002**, *106*, 2488.

(62) Kofranek, M.; Kovář, T.; Lischka, H.; Karpfen, A. *THEOCHEM* **1992**, *91*, 181.

(63) Greenwald, Y.; Cohen, G.; Poplawski, J.; Ehrenfreund, E.; Speiser, S.; Davidov, D. *J. Am. Chem. Soc.* **1996**, *118*, 2980.

(64) Greenwald, Y.; Poplawski, J.; Ehrenfreund, E.; Speiser, S. *Synth. Met.* **1997**, *85*, 1353.

(65) Cravino, A.; Zerza, G.; Neugebauer, H.; Maggini, M.; Bucella, S.; Menna, E.; Svensson, M.; Andersson, M. R.; Brabec, C. J.; Sariciftci, N. S. *J. Phys. Chem. B* **2002**, *106*, 70.

(66) Chakraborty, D.; Lagowski, J. B. *J. Chem. Phys.* **2001**, *115* (1), 184.

(67) Della Sala, F.; Heinze, H. H.; Görling, A. *Chem. Phys. Lett.* **2001**, *339*, 343.